

Why every electromagnetic inversion needs a 3D forward simulation

Lindsey J. Heagy¹, Douglas W. Oldenburg¹, Seogi Kang², and Dikun Yang³

<https://doi.org/10.1190/tle44110847.1>

Abstract

Modern electromagnetic (EM) surveys deliver high-quality data with broad spatial coverage and high spatial density, providing an opportunity to produce higher-quality images of the earth's subsurface than in the past. Because geologic structures are inherently 3D, the ultimate goal of an EM survey is to recover a 3D conductivity model that supports robust decision-making and interpretation. Nonetheless, practical inversion and interpretation workflows often still rely on simplifying assumptions, such as a 1D layered earth or parametric targets like plates. This paper illustrates the value of incorporating 3D forward simulation into the interpretation workflow. By running a forward simulation for the EM responses of inversion-derived models in full 3D, practitioners can assess the consistency of inversion results with the measured data and identify potential artifacts. Using two examples, namely, a dipping conductor and a porphyry-style deposit, we demonstrated how models that appear plausible under 1D assumptions fail under 3D scrutiny. Identifying areas where 1D assumptions fail can prompt additional analysis, such as iterative hypothesis testing or more focused 3D inversions. As such, 3D forward simulation should be considered an essential tool in the EM practitioner's toolbox.

Introduction

Variations in subsurface electrical conductivity are diagnostic for a wide range of geoscience and engineering problems that include mineral exploration, groundwater mapping, CO₂ sequestration, geothermal development, and environmental remediation. Because geologic structures are inherently 3D, the ultimate goal of an electromagnetic (EM) survey is to recover a 3D conductivity model that can guide decisions and interpretations.

Modern surveys now have the spatial coverage and data density needed to support that goal. Controlled-source EM systems that include airborne, ground-based, and borehole sensors routinely collect tens to hundreds of thousands of EM responses using tight line spacing, broad bandwidths, and diverse transmitter-receiver configurations. Airborne EM systems with mounted loops can collect data over a dense grid, and large-loop sources deployed on land can be paired with the surface or downhole receivers measuring electric or magnetic fields. DC resistivity and induced polarization

surveys collect electric field data with unstructured data acquisition locations, and magnetotelluric surveys likewise deploy grids of receivers or even continental-scale arrays (e.g., USArray [<https://www.earthscope.org/>] and AusLamp [<https://www.ga.gov.au/about/projects/resources/auslamp>]) to interrogate 3D geologic structures. These technological advances have made 3D resolution and images a realistic expectation, not a distant ideal.

Yet in practice, many data sets are still inverted using 1D or simplified 2D assumptions, or by representing the subsurface with a parametric geometry, to reduce computational demands and simplify the inversion for the user. These assumptions can produce reasonable results in some geologic settings. Moreover, industry-standard 1D inversions and plate modeling codes are efficient and widely used. However, in geologically complex settings, such simplifications risk misinterpreting targets of interest. This requires that the data be inverted using a full 3D formulation. Such codes exist, and there have been advancements to make them efficient. OcTree meshes allow for adaptive refinement within the areas of interest and for rapid coarsening of cells outside of this region to pad sufficiently to satisfy boundary conditions (Haber and Heldmann, 2007). Survey decomposition methods can be used to break up the forward simulation by source so that each can be computed in parallel on a mesh that has fewer cells than the global inversion mesh, speeding up the simulation and sensitivity computations (Cox et al., 2010; Haber and Schwarzbach, 2014; Yang and Oldenburg, 2016). With these approaches, problems that were previously intractable are now feasible. There are multiple codes that can be used for 3D inversion of time-domain EM (TDEM) data, and there have been multiple review papers on this topic (Macnae et al., 2012; Smith, 2014). Because EM inversions are nonlinear, each of the choices made in setting up the inversion can have important implications for the result obtained. The development of tutorials, training materials, and open-source codes are important avenues for helping to reduce the hurdles for 3D EM inversion. This work is in progress within the SimPEG project (Cockett et al., 2015; Heagy et al., 2017) and in other projects. However, it is still often the case that the required computational resources and expertise may not be available for every project.

Fortunately, while full 3D inversion remains challenging, 3D forward simulation is accessible, robust, and generally

Manuscript received 30 June 2025; revision received 12 August 2025; accepted 27 August 2025.

¹University of British Columbia, Geophysical Inversion Facility, Vancouver, Canada. E-mail: lheagy@eoas.ubc.ca; doug@eos.ubc.ca.

²University of Manitoba, Earth Sciences Department, Winnipeg, Canada. E-mail: sgkang09@stanford.edu.

³Southern University of Science and Technology, Department of Earth and Space Sciences, Shenzhen, China. E-mail: yangdikun@gmail.com.

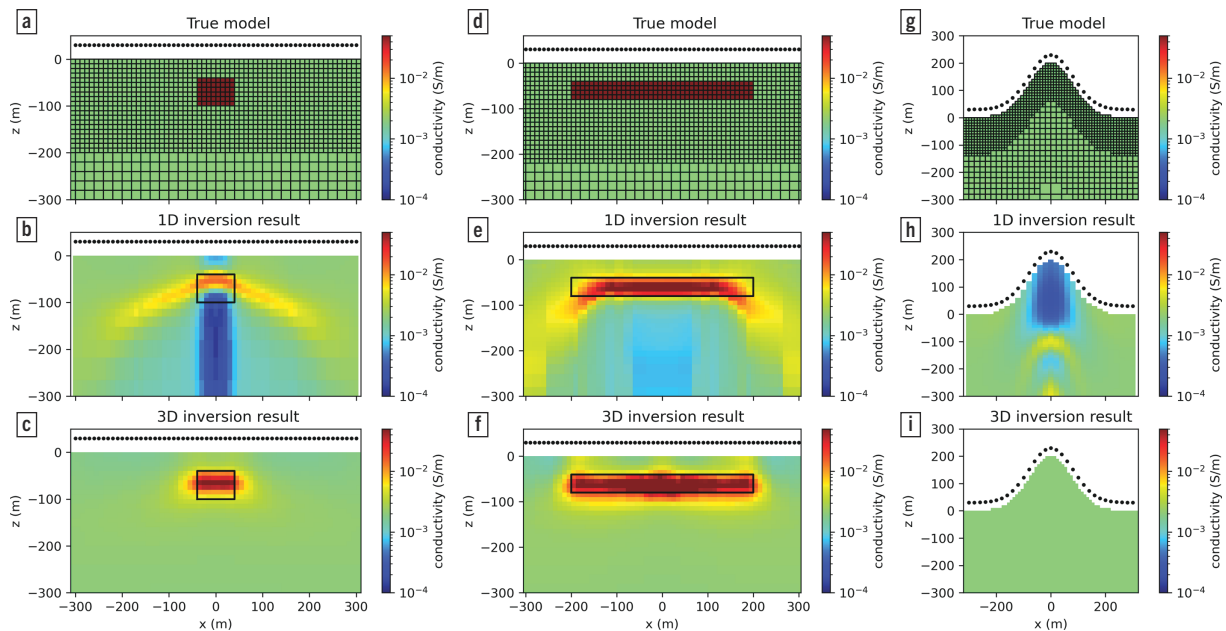


Figure 1. Examples of where 1D inversions can break down. The top row shows the true models of (a) a compact conductor, (b) a flat-lying conductor, and (c) a topographic feature with uniform, homogeneous conductivity. An OcTree mesh that is refined near the surface is used for all simulations. The black dots indicate the sounding locations used in the inversions. A step-off waveform is used, and 20 time channels from 2×10^{-2} to 2 ms are used for the respective 1D and 3D inversions (second and third rows, respectively).

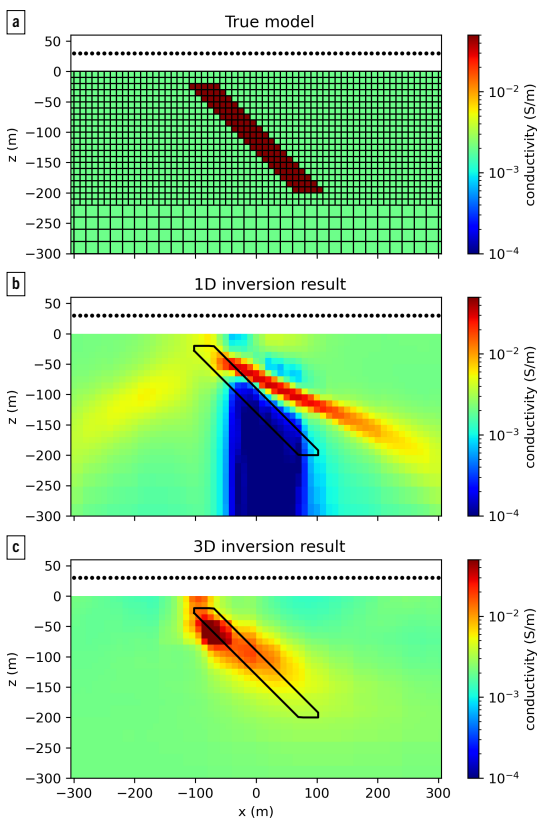


Figure 2. Inversion of Airborne Electromagnetic (AEM) data collected over a target with a dip of 45°. (a) True model. Black dots indicate sounding locations. (b) Model obtained through 1D inversion of data. (c) Model obtained through 3D inversion.

straightforward to implement. There are now many forward simulation codes, both proprietary and open-source, that are available (e.g., Börner et al., 2008; Cox et al., 2010; Yang and Oldenburg, 2016; Heagy et al., 2017; Rochlitz et al., 2019; Lu

and Farquharson, 2020, among others). Efforts to document, test, and develop tutorials for these codes help to train users. Carrying out a simulation provides a valuable check on whether a model that is obtained by 1D inversion, 2D inversion, or parametric fitting can actually reproduce the observed data when the full physics is applied. To illustrate the necessity of carrying out 3D simulations, we consider the inversion of airborne TDEM data. Typically, 1D inversion algorithms form the heart of the analysis. These inversions are typically quite fast to perform, and there are a variety of well-established algorithms that are trusted by industry (e.g., Farquharson and Oldenburg, 1993; Viezzoli et al., 2008; Brodie and Richardson, 2015; Kang et al., 2018, among others).

In Figure 1, we show examples of common “failure modes” of 1D airborne EM inversions. Over a compact conductor (Figure 1a), a 1D inversion will recover “pant-leg” conductive structures as well as a resistor beneath the target. Similar artifacts can be seen when a flat-lying target is present (Figure 1d). If topography is present, 1D inversions will tend to recover a resistor underlain by a conductor within the topography feature. Each of these artifacts arises because the assumption of a 1D earth is being broken, whereas a 3D inversion can accurately account for such effects (Figure 1c, 1f, and 1i).

This paper illustrates the value of incorporating 3D forward simulation into the interpretation workflow. We use the UBC-GIF TD OcTree tiled code (Haber and Schwarzbach, 2014), as well as the 1D and 3D SimPEG time-domain codes in our analysis (Heagy et al., 2017; Kang et al., 2018). By simulating the responses of inversion-derived models in 3D, one can quickly assess the internal consistency of results and identify problematic artifacts. Through two examples, a dipping conductor and a porphyry-style deposit, we

demonstrate how models that appear plausible in 1D fail under 3D scrutiny. This approach enables iterative hypothesis testing, helps guide targeted 3D inversion, and ultimately improves the reliability of geophysical interpretations.

Example 1: Dipping target

The first example we consider is the dipping target, shown in Figure 2. The target has a conductivity of 0.05 S/m ($20\ \Omega\text{m}$) and is embedded in a 0.002 S/m (500 Ωm) half-space. The target has a dip of 45° and extends from $y = -400$ to 400 m. We simulate a single line of data with a 10 m loop source at a height of 30 m above the surface. The along-line spacing is 20 m and the line extends from $x = -300$ to 300 m. We

use a step-off waveform and measure the vertical component of db/dt at 20 time channels from 2×10^{-2} to 2 ms. The 1D inversions are each independent and no lateral or spatial constraints are included. For the 3D inversion, we use a large α_y value to recover a structure that is approximately 2D (very smooth in the y -direction, which is oriented into the page). The 1D and 3D recovered models are shown in Figure 2b and 2c, respectively.

The 1D inversion recovers a dipping target, but the recovered dip (approximately 30°) is shallower than the true dip (approximately 45°) and the recovered target extends further in the down-dip direction, extending out to nearly $x = 200$ m, whereas the true target only extends to $x = 100$ m. There are other notable inversion artifacts, including the strong resistor beneath the target, as well as a fainter conductive artifact that extends from the top of the target to $x = -200$ m. The 3D inversion recovers the correct dip and location of the target, although not its full extent at depth, as we lose resolution with depth as the currents diffuse downward and outward.

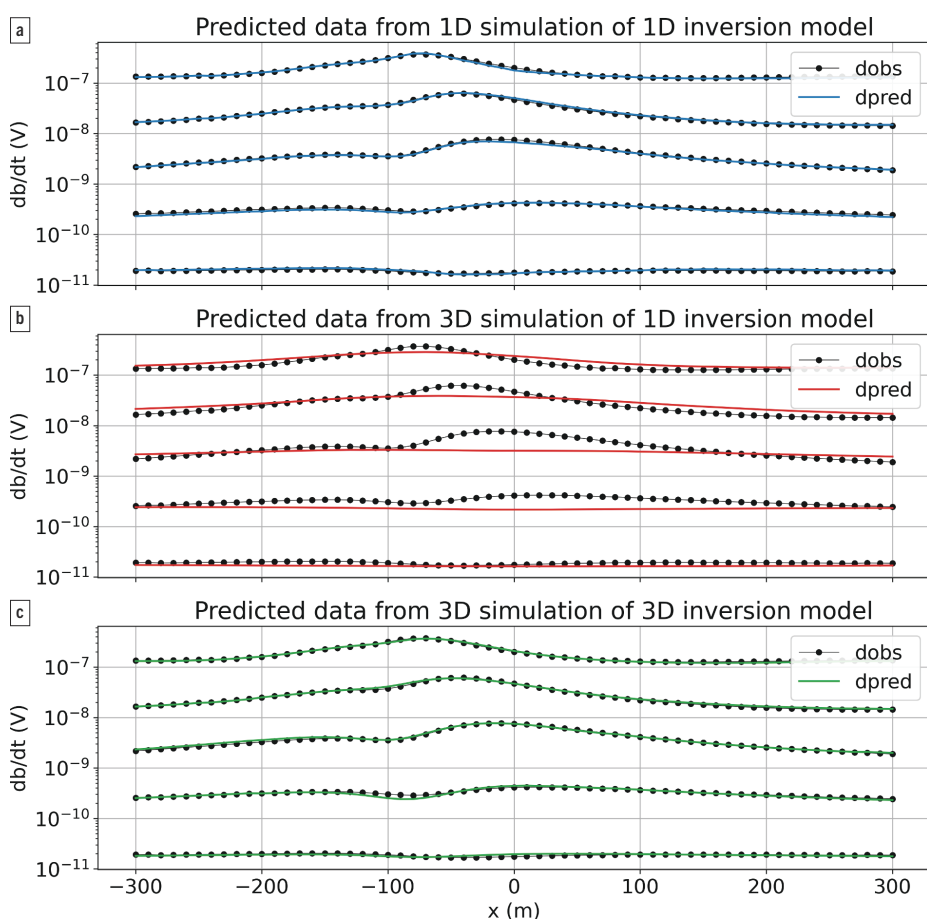


Figure 3. Plots of the observed and predicted data for every 4th time channel. (a) 1D simulations performed over the 1D inversion result. (b) 3D simulation performed over the 1D inversion result. (c) 3D simulation performed over the 3D inversion result.

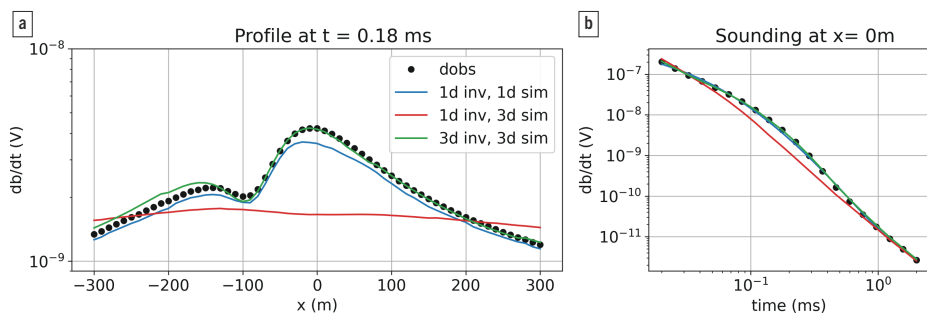


Figure 4. Predicted and observed data for (a) a profile at $t = 0.18$ ms and (b) a single sounding at $x = 0$ m.

(Figure 3c, green lines), however, fits the data well and has a reasonable recovery of the target because it fully simulates the 3D physics.

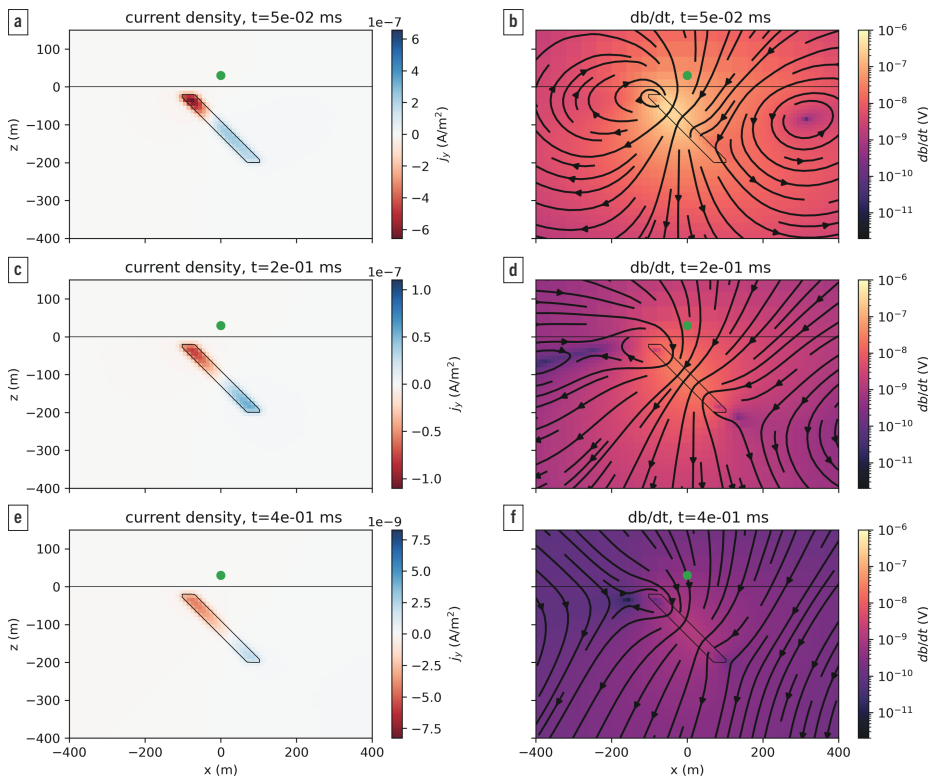


Figure 5. Plots of the current density (left) and db/dt (right) fields at three different times for a source at $x = 0 \text{ m}$, $z = 30 \text{ m}$ (green dot).

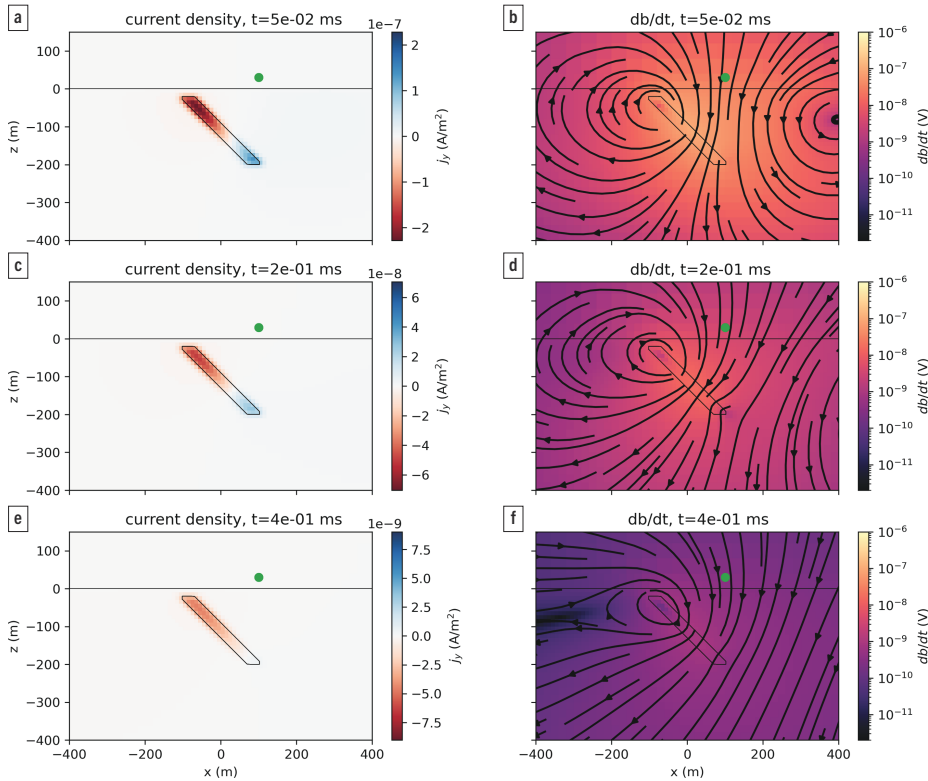


Figure 6. Plots of the current density (left) and db/dt (right) fields at three different times for a source at $x = 100 \text{ m}$.

To illustrate how the 1D assumption breaks down, it can be insightful to look at the EM fields through time. Figure 5 shows the current density (left) and db/dt field (right) through time for the sounding located at $x = 0 \text{ m}$. At early times, we see strong current density values near the up-dip portion of the target. The 1D inversion needs to explain the resulting db/dt measurements, so it brings the conductive layer shallower. The currents reach the edges of the target in the mid-to-late times, which cannot be accounted for in a 1D inversion that assumes that the layer extends laterally to infinity. The inversion tries to explain the data by introducing a strong resistor underneath the conductive target. For an offset source, such as at $x = 100 \text{ m}$, we can again gain insights into the artifacts produced by the 1D inversion by looking at the fields shown in Figure 6. Although the source is not over the target, it is still close enough to couple with it and induce currents. As a result, this sounding produces a db/dt response that can be measured and needs to be explained by the recovered model at that location.

Example 2: Synthetic model inspired by Mt. Milligan deposit

Mt. Milligan is an alkalic porphyry Cu–Au deposit located approximately 155 km northwest of Prince George in British Columbia, Canada. It lies within the Early Mesozoic Quesnel Terrane, where many similar porphyry deposits have been discovered (DeLong et al., 1990; Oldenburg, Li, and Ellis, 1997). In 2007, a versatile time domain electromagnetic (VTEM) survey was flown over the deposit as a part of the Geoscience BC QUEST project. Yang and Oldenburg (2012) inverted these data in 3D to produce a model that agreed well with the known geologic information from drilling. They also developed a synthetic example to illustrate the pitfalls of 1D inversion for this geologic model. Here, we revisit the synthetic model first presented in Yang and Oldenburg (2012).

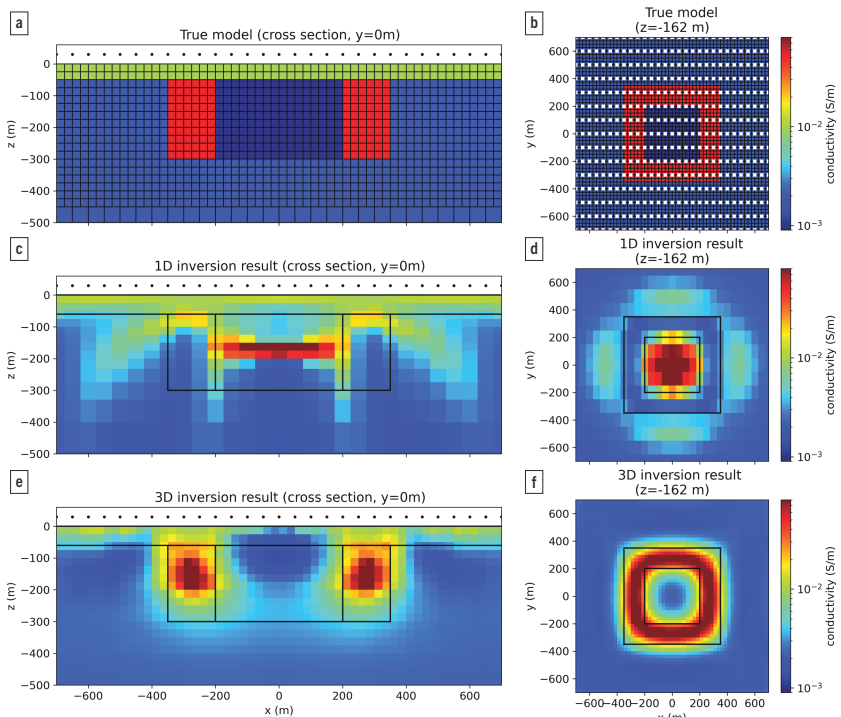


Figure 7. Synthetic model inspired by the Mt. Milligan deposit (after Yang and Oldenburg, 2012). (a) Cross-section through the true model. (b) Depth slice of the true model at $z=162$ m. White dots indicate sounding locations. (c and d) Cross-section and depth slice through the model recovered using 1D inversion. (e and f) Cross-section and depth slice through the model recovered using 3D inversion.

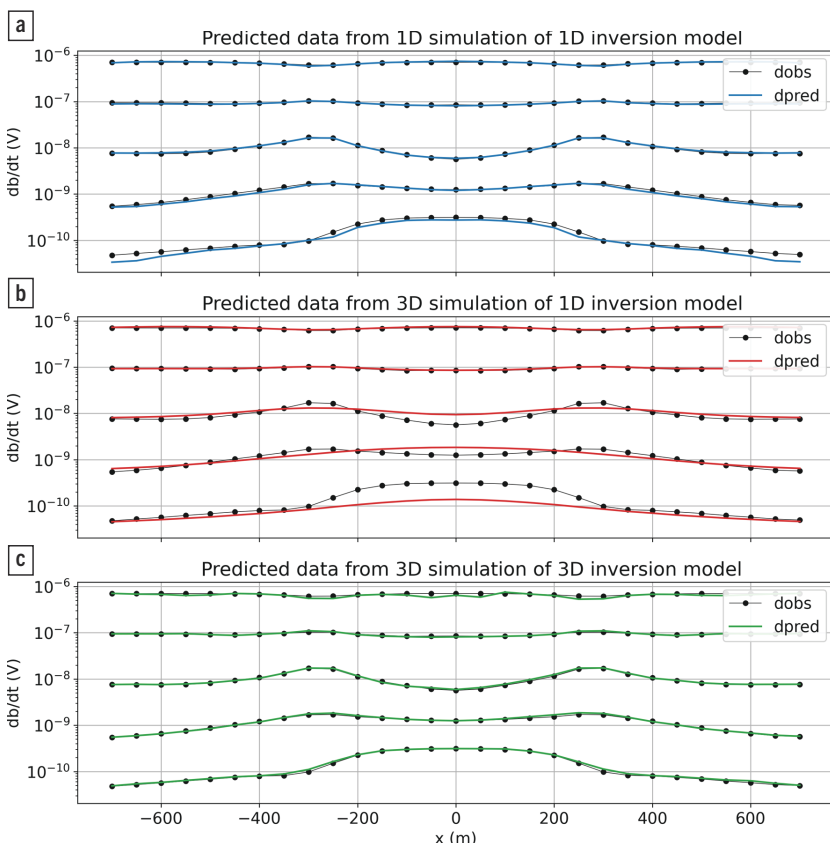


Figure 8. Plots of the observed and predicted data for every 4th time channel along the $y=0$ m line for the Mt. Milligan example. (a) 1D simulations performed using the model obtained from the 1D inversion. (b) 3D simulation performed over the model obtained from 1D inversion. (c) 3D simulation performed with the model obtained through 3D inversion.

The model is shown in Figure 7a as a cross-section, and Figure 7b shows a depth slice. We use mesh cells that are $50 \times 50 \times 25$ m. The overburden is 50 m thick and has a resistivity of $10 \Omega\text{m}$ (0.01 S/m). The background is $500 \Omega\text{m}$. The deposit consists of two regions. The inner portion is a resistive ($1000 \Omega\text{m}$) stock that hosts the mineralization. Surrounding the resistive stock is an altered region that is more conductive ($20 \Omega\text{m}$). We simulate a higher-density survey than Yang and Oldenburg (2012) and use a line spacing of 100 m. Along each line, we use soundings that are 50 m apart for the inversions.

The models obtained by inverting the data in 1D and 3D are shown in Figure 7c–f. These models tell two very different geologic stories. The 1D inversion recovers a conductor where the resistive core should be, whereas the 3D inversion recover the resistive core and conductive altered halo that hosts the mineralization.

In Figure 8, we show a comparison of the “observed” data from the 3D simulation along with the predicted data from the inverted models. Figure 8a shows the data predicted by 1D simulations of each sounding from the 1D inversion model. The data are well-fit in the inversion. However, when we interpolate this model onto a 3D Octree mesh and perform a 3D simulation, we see that the predicted data are a poor representation of the observed data, particularly in the mid and late times over the deposit, as shown in Figure 8b. The 3D inversion result fits the observed data at all time channels (Figure 8c).

In Figure 9, we plot a profile of a single time channel (Figure 9a) and a single sounding at $x = 0$ m (Figure 9b), with all results together to compare. While the 1D inversion model appears to fit the data when simulated with a 1D algorithm, when we simulate the 1D model with a 3D algorithm, we see that the anomaly produced has a completely different character than

the observed data. It can also be insightful to look at misfit maps, which we show for a single time channel in Figure 10. Again, we see that the character of the anomaly produced by the 1D model is completely different from the predicted data, and in the misfit plot in Figure 10c, we see a coherent structure that is similar in character to the true data in Figure 10a, which should serve as a red flag for interpreters.

To help understand how the 1D assumption breaks down for this example, we show the currents and db/dt fields for a sounding

over the center of the deposit in Figure 11. Currents concentrate in the conductive altered zone, and the 1D inversion explains the db/dt response by putting a conductor beneath the sounding location. This happens for offset soundings as well. In Figure 12, we simulate a sounding at the interface between the resistive stock and the conductive alteration halo ($x = 200$ m, $y = 0$ m). At early times, the currents are concentrated in the conductive altered zone closest to the transmitter. At later times, the currents have diffused further and circulate through the whole altered zone, similar to

when the sounding was at the center of the deposit. These effects are highly 3D, but the 1D inversion can fit the sounding by again putting a conductive unit beneath the transmitter.

The two examples presented, a dipping target and a deposit model inspired by the Mt. Milligan porphyry deposit, illustrate where 1D inversion produces misleading results that could lead to incorrect interpretations. For the example of the dipping target, we showed that the recovered dip of approximately 30° was much shallower than the true dip of 45°, and the target appears to extend further along the profile than it does in reality. For the Mt. Milligan example, the 1D inversion model leads to an entirely different interpretation, as pointed out by Yang and Oldenburg (2012). It shows a conductive structure where the resistive core is and places a shallow conductor where the altered halo that the mineralization should be. In both examples, the 1D inversions can fit the data well when each sounding is simulated in 1D. If this is the only metric used to assess the quality of the result, there is a large risk of placing false confidence in that model. This can lead to costly mistakes in drilling or in choosing whether to further develop a property or to let it go.

By taking the model obtained through 1D inversion, interpolating it onto a 3D mesh, and performing a 3D forward simulation, we can test whether that model produces data that are similar to the observed data or not. The data fit can be quantified by a single number, the data misfit, but it is important to look at profiles and maps. By looking at profiles and maps of

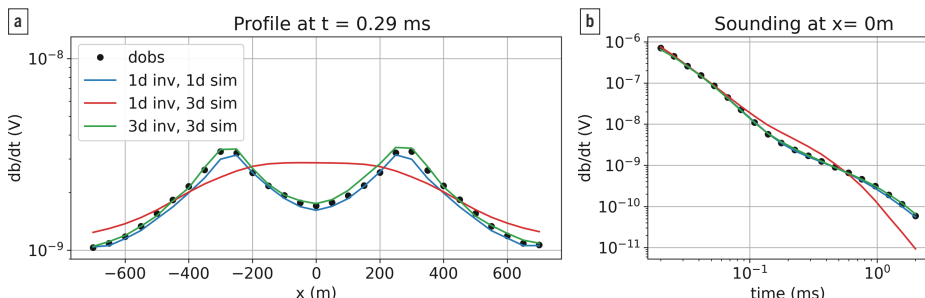


Figure 9. Predicted and observed data for (a) a profile at $t = 0.29$ ms and (b) a single sounding at $x = 0$ m, $y = 0$ m. The source is at $z = 30$ m.

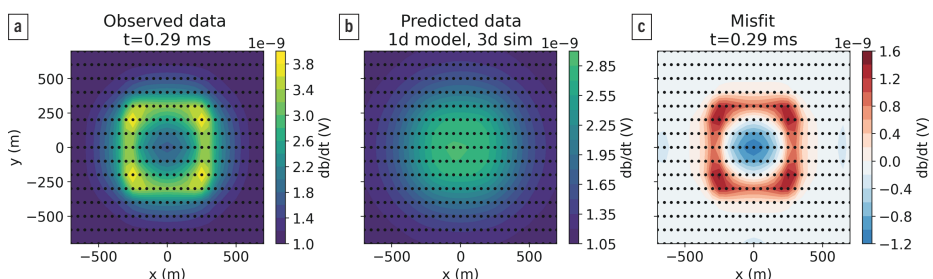


Figure 10. Time slice of data (a) observed data from the true model, (b) data computed by a 3D simulation of the model obtained through 1D inversion, and (c) misfit (observed–predicted).

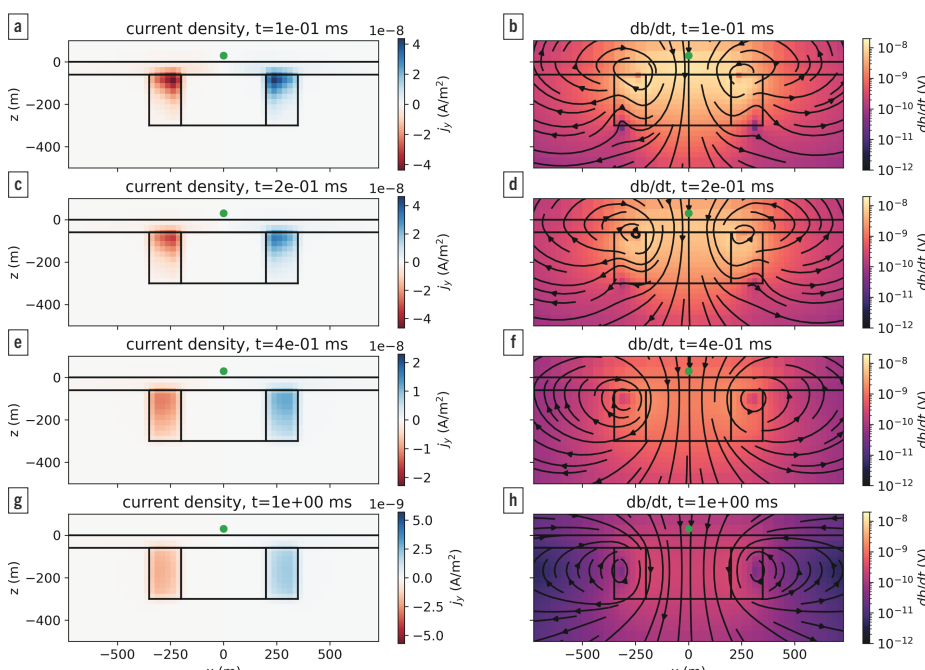


Figure 11. Plots of the current density (left) and db/dt (right) fields at three different times for a source at $x = 0$ m for the Mt. Milligan example.

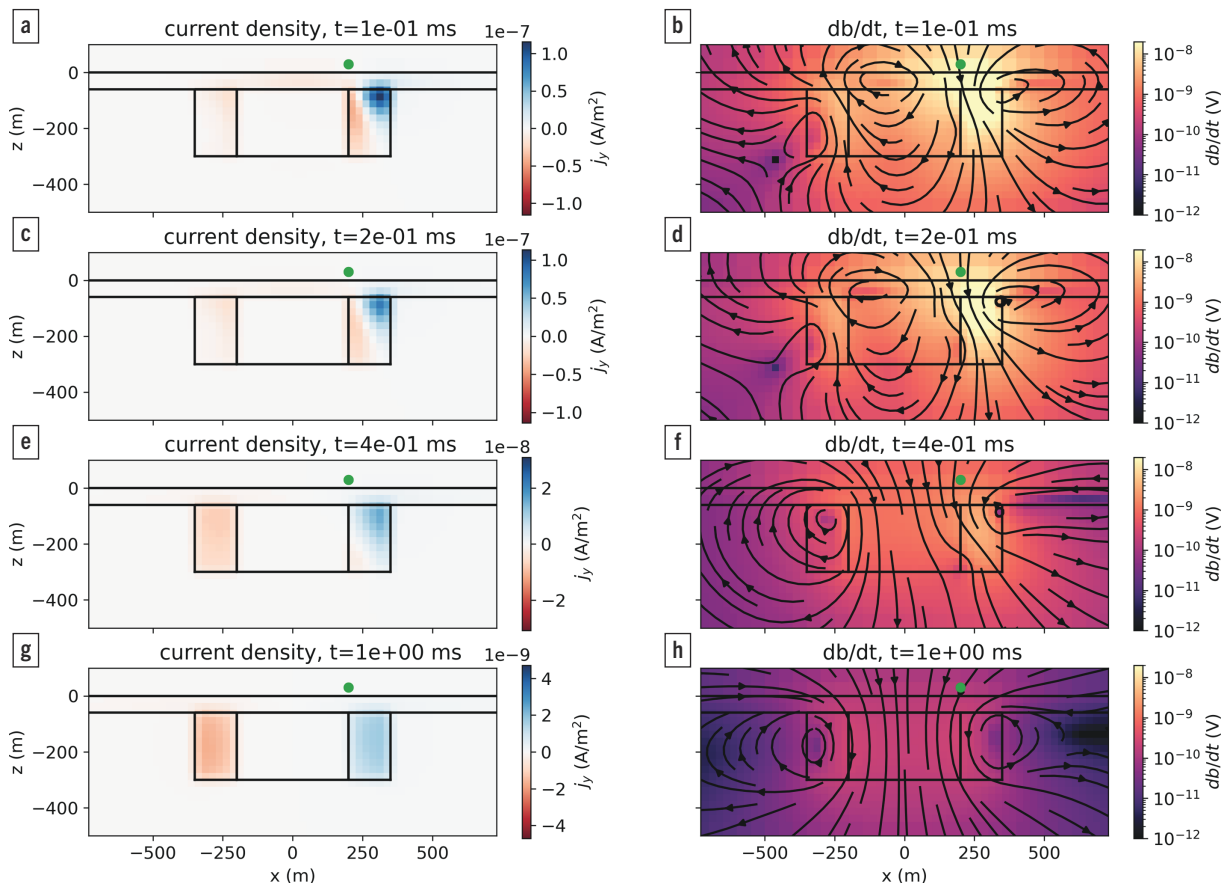


Figure 12. Plots of the current density (left) and db/dt (right) fields at three different times for a source at $x=200$ m, $y=0$ m for the Mt. Milligan example.

individual time channels and their misfits, we can identify problematic regions and areas with coherent signals that are not being fit. This should prompt questions and further analysis for features of interest. Hypothesis testing can be performed by simplifying the model and running forward simulations, for example, testing if a compact conductor at the center of the Mt. Milligan survey area, in fact, fits the data. This can be followed up with 3D inversions on subsets of the data. Forward simulations in 3D can be even more important when 3D survey geometries are used and the data are less intuitive to interpret (Cheng et al., 2023).

Conclusions

Modern EM surveys routinely deliver high-quality data sets with dense spatial coverage, enabling detailed imaging of the subsurface. Yet, despite these extensive data, interpretation is often carried out by invoking simplifying assumptions, such as treating the subsurface as a 1D layered earth or approximating targets as conductive plates. While these assumptions reduce computational cost and are often sufficient in layered settings, they can introduce significant artifacts when applied to complex geology. Critically, the apparent success of these inversions in fitting the data does not guarantee that the resulting model is physically plausible in 3D.

This is where 3D forward simulation becomes indispensable. By applying full 3D physics to models derived from simpler

assumptions, practitioners can test whether these models genuinely reproduce the observed data. When discrepancies arise, they can reveal where further refinement, hypothesis testing, or targeted 3D inversion is warranted. With a growing ecosystem of open-source and proprietary simulation tools, along with improving tutorials and community support, 3D forward simulation is increasingly accessible. It should be embraced as a routine step in EM interpretation workflows, not just for advanced users but for anyone aiming to produce reliable, decision-ready subsurface models. **TLE**

Acknowledgment

The authors are grateful to the two anonymous referees who took the time to help improve the quality of this manuscript.

Data and materials Availability

Data associated with this research are available and can be accessed via the following URL: <https://github.com/ubcgif/2025-heagy-etal-tle>

Corresponding author: lheagy@eoas.ubc.ca

References

- Börner, R. U., O. G. Ernst, and K. Spitzer, 2008, Fast 3-D simulation of transient electromagnetic fields by model reduction in the frequency domain using Krylov subspace projection: Geophysical

- Journal International, **173**, no. 3, 766–780, <https://doi.org/10.1111/j.1365-246X.2008.03750.x>.
- Brodie, R. C., and M. Richardson, 2015, Open source software for 1D airborne electromagnetic inversion: ASEG Extended Abstracts, **2015**, no. 1, 1–3, <https://doi.org/10.1071/ASEG2015ab197>.
- Cheng, M., D. Yang, and Q. Luo, 2023, Interpreting surface large-loop time-domain electromagnetic data for deep mineral exploration using 3D forward modeling and inversion: Minerals, **13**, no. 1, 34, <https://doi.org/10.3390/min13010034>.
- Cockett, R., S. Kang, L. J. Heagy, A. Pidlisecky, and D. W. Oldenburg, 2015, SimPEG: An open source framework for simulation and gradient based parameter estimation in Geophysical Applications: Computers & Geosciences, **85**, 142–154, <https://doi.org/10.1016/j.cageo.2015.09.015>.
- Cox, L. H., G. A. Wilson, and M. S. Zhdanov, 2010, 3D inversion of airborne electromagnetic data using a moving footprint: Exploration Geophysics, **41**, no. 4, 250–259, <https://doi.org/10.1071/EG10003>.
- DeLong, R. C., C. I. Godwin, M. W. Harris, N. M. Caira, and C. M. Rebagliati, 1990, Geology and alteration at the mount milligan gold-copper porphyry deposit. Central British Columbia (93N71E), Geological Fieldwork, <https://propertyfile.gov.bc.ca/reports/PF885720.pdf>.
- Farquharson, C. G., and D. W. Oldenburg, 1993, Inversion of time-domain electromagnetic data for a horizontally layered Earth: Geophysical Journal International, **114**, no. 3, 433–442, <https://doi.org/10.1111/j.1365-246X.1993.tb06977.x>.
- Haber, E., and S. Heldmann, 2007, An octree multigrid method for Quasi-Static Maxwell's equations with highly discontinuous coefficients: Journal of Computational Physics, **223**, no. 2, 783–796, <https://doi.org/10.1016/j.jcp.2006.10.012>.
- Haber, E., and C. Schwarzbach, 2014, Parallel inversion of large-scale airborne time-domain electromagnetic data with multiple OcTree meshes: Inverse Problems, **30**, no. 5, 055011, <https://doi.org/10.1088/0266-5611/30/5/055011>.
- Heagy, L. J., R. Cockett, S. Kang, G. K. Rosenkjaer, and D. W. Oldenburg, 2017, A framework for simulation and inversion in electromagnetics: Computers and Geosciences, **107**, 1–19, <https://doi.org/10.1016/j.cageo.2017.06.018>.
- Kang, S., D. Fournier, D. Werthmuller, L. J. Heagy, and D. W. Oldenburg, 2018, SimPEG-EM1D: Gradient-based 1D inversion software for large-scale airborne electromagnetic data. In AGU Fall Meeting Abstracts, 2018: NS53A–0557.
- Lu, X., and C. G. Farquharson, 2020, 3D finite-volume time-domain modeling of geophysical electromagnetic data on unstructured grids using potentials: Geophysics, **85**, no. 6, 221–240, <https://doi.org/10.1190/geo2020-0088.1>.
- Macnae, J., K. Witherly, and T. Munday, 2012, 3D EM inversion: An update on capabilities and outcomes: Preview, **159**, 24–27, <https://doi.org/10.1071/PVv2012n159p24>.
- Oldenburg, D. W., Y. Li, and R. G. Ellis, 1997, Inversion of geophysical data over a copper gold porphyry deposit: A case history for Mt. Milligan: Geophysics, **62**, 1419–1431, <https://doi.org/10.1190/1.1444246>.
- Rochlitz, R., N. Skibbe, and T. Günther, 2019, custEM: Customizable finite-element simulation of complex controlled-source electromagnetic data: Geophysics, **84**, no. 2, F17–F33, <https://doi.org/10.1190/geo2018-0208.1>.
- Smith, R., 2014, Electromagnetic induction methods in mining geophysics from 2008 to 2012: Surveys in Geophysics, **35**, no. 1, 123–156, <https://doi.org/10.1007/s10712-013-9227-1>.
- Viezzoli, A., A. V. Christiansen, E. Auken, and K. Sørensen, 2008, Quasi-3D modeling of airborne TEM data by spatially constrained inversion: Geophysics, **73**, no. 3, F105–F113, <https://doi.org/10.1190/1.2895521>.
- Yang, D., and D. W. Oldenburg, 2012, Three-dimensional inversion of airborne time-domain electromagnetic data with applications to a porphyry deposit: Geophysics, **77**, no. 2, B23–B34, <https://doi.org/10.1190/geo2011-0194.1>.
- Yang, D., and D. W. Oldenburg, 2016, Survey decomposition: A scalable framework for 3D controlled-source electromagnetic inversion: Geophysics, **81**, no. 2, E69–E87, <https://doi.org/10.1190/GEO2015-0217.1>.